Research Paper

Acoustic Attenuation Performance Analysis and Optimisation of Expansion Chamber Coupled Micro-perforated Cylindrical Panel Using Response Surface Method

Mohamad Izudin ALISAH(1), Lu Ean OOI(1)*, Zaidi Mohd RIPIN(1), Ahmad Fadzli YAHAYA(2), Kelvin HO(2)

(1) *The Vibration Lab, School of Mechanical Engineering, Engineering Campus, Universiti Sains Malaysia*
14300 Nibong Tebal, Pulau Pinang, Malaysia
*Corresponding Author e-mail: ooiluean@usm.my

(2) *Dyson Manufacturing*
81400 Senai, Johor, Malaysia

(*received August 14, 2020; accepted February 4, 2021*)

This paper describes the boundary element method (BEM) and the experimental and optimisation studies conducted to understand the potential of expansion chamber coupled micro-perforated cylindrical panel (MPCP) in enhancing the acoustic attenuation for in-duct noise control issues. Owing to the complex structure of the MPCP and to achieve the correct prediction of acoustic attenuation, BEM is adopted on the basis of the Simcenter 3D software to compute the sound transmission loss (TL), As the MPCP is cylindrical in shape with numbers of sub-milimeter holes, additive manufacturing-based 3D printing is utilised for the model prototyping to reduce current design limitation and enable fast fabrication. The TL measurement-based two-load method is adopted for model validation. Subsequently, parametric studies of the MPCP concerning the perforation hole diameter, perforation ratio and depth of air space are carried out to investigate the acoustic performance. Optimisation via response surface method is used as it allows for evaluating the effects of multiple parameters as required in this study. The model validation result shows that the error between the BEM and the measured values is relatively small and shows good agreement. The R-square value is 0.89. The finding from the parametric studies shows that a wider peak attenuation can be achieved by reducing the perforation hole diameter, and one way to increase the TL amplitude is by increasing the air cavity depth. Finally, the optimised MPCP model is adopted to the commercial vacuum cleaner for verification. The sound pressure level of the vacuum cleaner is significantly attenuated within the objective frequency of 1.7 kHz.

Keywords: micro-perforated cylindrical panel; transmission loss; boundary element method; response surface method.

1. Introduction

The acoustic behaviour of an expansion chamber with absorbing material improves its acoustic performance (Delany, Bazley, 1970; Na *et al.*, 2007), However, for applications that need clean absorbent with high air flux, conventional porous absorbers use is inappropriate. Therefore, micro-perforated panel (MPP) has been proposed recently to remove the usage restriction and achieve broadband frequency attenuation (Qian *et al.*, 2013; Tan, Ripin, 2016; Ren *et al.*, 2019).

Currectly, the main research methods for predicting the acoustic performance of the expansion chamber include transfer matrix method (TMM), finite element method (FEM) and boundary element method (BEM), Munjal (1987) applied the TMM-based 1D plane wave theory for several acoustic elements and silencer configurations. The simplistic approach yields good agreement at lower frequency yet deviates from experimental results at higher frequency. Thus, a multi-dimensional method is required for accurate acoustic attenuation prediction. Fu *et al.* (2015) used FEM to

simulate the transmission loss (TL) of the exhaust muffler. The study adopted an automatic matched layer method to simulate the non-reflecting boundary condition in order to avoid a complex calculation. The results showed the error between FEM and measured value is small at frequencies smaller than 3000 Hz. Tan and Ripin (2013) investigated the effect of the MPP inside the expansion chamber by using BEM. The model was verified with the impedance tube measurement and showed good agreement. The accuracy was improved by 40% in the BEM model compared to that in the analytical approach.

As the micro-perforated cylindrical panel (MPCP) model used in this study is cylindrical in shape, BEM is thus adopted for the simulation purpose as it is capable of simulating a complex structure with high acoustic precision (Selamet *et al.*, 1998; Selamet, Ji, 1999). Subsequently, the BEM approach for acoustic models can be developed through the link to CAD, resulting in a straightforward boundary mesh generation compared with volume mesh generation. It can be completed automatically with little user interaction (Citarella, Landi, 2011). BEM also offers better performance for the exterior problem and reduces the dimensionality of the meshing domain when considering the complex geometry of the complex components (Citarella, Landi, 2011). Literature shows the BEM approach is widely used in the simulation on silencers for predicting its attenuation performance (Zhenlin *et al.*, 1994). In general, BEM is able to perform good prediction and results in close agreement with measurements (Ji, Selamet, 2000).

Traditionally, MPP has been fabricated by metal through hole drilling or laser cut process. In the case of a complex structure with numbers of sub-milimeter holes of the MPCP model, 3D printing based on additive manufacturing (AM) is more convenient. With the recent technologies in AM, it can reduce current design limitations and enable fast prototyping of the MPCP. Thus, the MPCP model can be printed within a reasonable time and price. Liu *et al.* (2017) utilised 3D printing technology to produce 0.6 mm holes of the multilayer MPP absorber (MPPA), The measured sound absorption coefficients matched well with the predicted values. Recently, Lu *et al.* (2019) manufactured the optimised structure of a compact MPP muffler using 3D printing technologies for experimental verification. The measured model shows good agreement with TMM predictions.

This study also investigates the combined effects of perforation hole diameter, perforation ratio and depth of air cavity of the MPCP model and optimises the process parameters by using central composite design (CCD) in conjunction with response surface method (RSM), RSM is utilised because it allows for evaluating the effects of multiple parameters and their interactions on one or more responses as required in the present research. Qin *et al.* (2016) used RSM to determine the optimal structural acoustics of an enclosed box-damped structure. The result indicates that, through the use of RSM, the sound pressure of the target node is controlled effectively and less damping material used. The computational time for the structural-acoustic system is shortened, and the optimisation process is simplified. Li and Liang (2007) utilised RSM to optimise the vibroacoustic properties of a damping structure and reduce its sound radiation. The optimisation process of the sound radiation level for the vibrating panel is carried out efficiently, and RSM provides clear direction for the design modification. Wang *et al.* (2017) investigated the structural-borne acoustic analysis enclosed box structure by using panel acoustic participation and applying RSM for multi-objective optimisation. The finding shows that the structural-borne acoustics at critical frequencies are calculated effectively. Subsequently, RSM optimisation is also applied to attenuate the sound pressure level (SPL) inside the passenger cabin (Yuksel *et al.*, 2012). In general, the result shows that the performance of optimum configurations is better compared to that of the baseline configuration. Finally, RSM is used in many applications such as vibration control (Ganguli, 2002; Kallias, Imran Rafiq, 2013) and advance manufacturing technology (Leong *et al.*, 2013; Aziz *et al.*, 2015; Ishak *et al.*, 2019).

The purpose of the present study is to simulate the MPCP model using BEM to compute the TL. The next is to investigate the acoustic attenuation effect of the perforation diameter, perforation ratio and depth of air cavity of the MPCP model. Finally, this study examines the optimal design of the MPCP model by utilising RSM and applying it to the commercial vacuum cleaner.

2. Theory

In this study, BEM is employed for predicting the acoustic attenuation performance of the expansion chamber coupled MPCP. Figure 1 illustrates the discussed model substructures, including inlet tube,

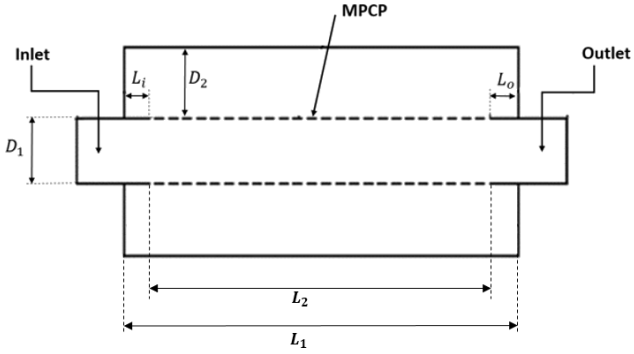

Fig. 1. A schematic diagram of the expansion chamber coupled MPCP model.

MPCP and outlet tube. The main parameters include inner diameter D_1, air cavity depth D_2 and expansion chamber whole length L_1, L_i, L_2, and L_o are the inlet unperforated length, perforated length and outlet unperforated length, respectively.

2.1. Three-point method

This study adopted BEM analysis on the basis of the Simcenter 3D, which employed the three-point method to predict the TL. As shown in Fig. 2, two arbitrary points (points 1 and 2) in the inlet tube and one arbitrary point (point 3) in the outlet tube were selected. Plane-wave motion was assumed in both inlet and outlet tubes. Given that the outlet tube has an anechoic termination, the acoustic wave in the outlet tube contained only an outgoing wave. The acoustic wave in the inlet tube contained an incoming wave and a reflected wave.

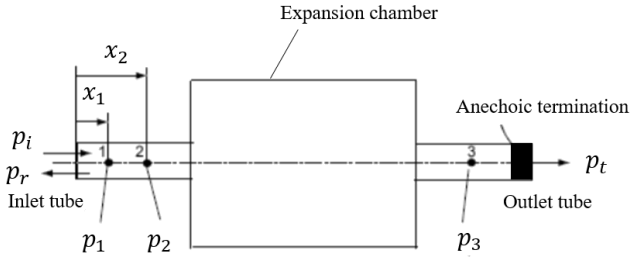

Fig. 2. The three-point method.

The corresponding sound pressures at p_1 and p_2 at the two points can be written as

$$p_1 = p_i e^{ikx_1} + p_r e^{-ikx_1}, \tag{1}$$

$$p_2 = p_i e^{ikx_2} + p_r e^{-ikx_2}, \tag{2}$$

where p_i represents the incoming wave, and $p_r$represents the reflected waves. Solving Eqs (1) and (2) for p_i gives the following:

$$p_i = \frac{1}{2i\,\sin[k\,(x_1 - x_2)]}(p_1 e^{-ikx_2} - p_2 e^{-ikx_1}), \tag{3}$$

provided that $\sin[k\,(x_1 - x_2)] \neq 0$ and $i^2 = -1$. TL is defined as the difference between the incoming sound power level and the outgoing sound power level, that is,

$$\mathrm{TL} = 20\log\frac{W_i}{W_o}, \tag{4}$$

where W_i is the incoming sound power and W_o is the outgoing sound power. Since the sound power of a plane wave is proportional to the square of the sound pressure amplitude and the tube cross-sectional area, Eq. (4) becomes

$$\mathrm{TL} = 20\log\frac{|p_i|}{|p_3|} + 10\log\frac{S_i}{S_o}. \tag{5}$$

2.2. Acoustic impedance of perforates

Figure 3 shows the basic construction of an MPPA, which comprises perforation hole diameter d, perforation spacing b, panel thickness t and air cavity depth D.

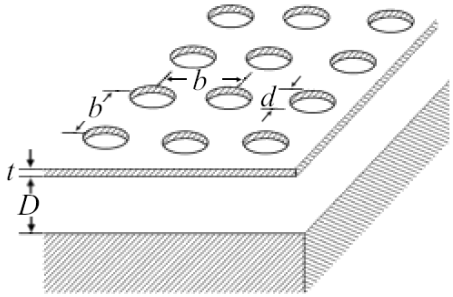

Fig. 3. Schematic diagram of MPP (Lu *et al.*, 2019).

According to Maa (1975), the specific acoustic impedance of a perforation can be expressed as

$$Z = R + j\omega M, \tag{6}$$

with

$$R = \frac{32nt}{d^2}\left[\sqrt{1 + \frac{k^2}{32}} + \frac{k\sqrt{2}}{8}\frac{d}{t}\right], \tag{7}$$

$$\omega M = \omega\rho_0 t\left[1 + \frac{1}{\sqrt{9 + \frac{k^2}{2}}} + 0.85\frac{d}{t}\right], \tag{8}$$

and

$$k = \frac{d}{2}\sqrt{\frac{\omega\rho_0}{n}}, \tag{9}$$

where R and ωM represent the perforation-specific acoustic resistance and acoustic reactance, respectively. n, ρ_o and ω represent the dynamic viscosity, air density and angular frequency of the incident acoustic wave, respectively. The relative acoustic of the perforate impedance is calculated as

$$\zeta_p = \frac{Z}{c\sigma\rho_0}, \tag{10}$$

where c and σ are the sound speed and panel perforation ratio, respectively.

3. Methodology

3.1. BEM simulation

As shown in Fig. 1, the MPCP was fitted in the expansion chamber. The geometry of the 3D MPCP model was developed on the basis of NX Nastran software. The model was then discretised into small surface elements by using the meshing tool in the software for subsequent BEM acoustic analysis, as illustrated in Fig. 4a.

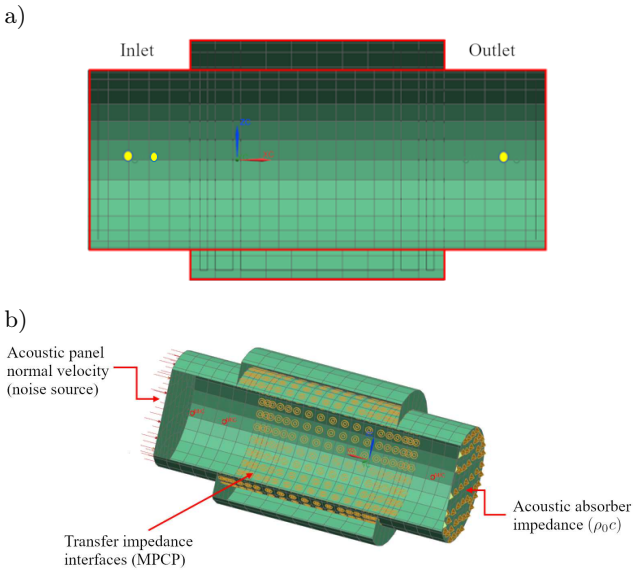

Fig. 4. a) The meshing model of the MPCP; b) cross-section view of expansion chamber coupled MPCP model.

In the BEM simulation, the fluid material properties of the model were defined as air, whose mass density was 1.225 $\mathrm{kg \cdot m^{-3}}$, and the sound speed was 340 $\mathrm{m \cdot s^{-1}}$. At the inlet of the main tube, the noise source of 1 $\mathrm{m \cdot s^{-1}}$ was modelled as the acoustic panel normal velocity (Vasile, 2010). At the outlet tube, the anechoic termination condition could be achieved by inserting the acoustic absorber impedance ($\rho_0 c$) value of 416.5 $\mathrm{kg \cdot m^{-2} \cdot s^{-1}}$. In this BEM model, the MPCPs were connected using the transfer impedance interfaces calculated according to Eqs (5)–(9), as illustrated in Fig. 4b. The point set mesh primitive was used to determine the SPL of the inlet and outlet tubes to obtain the TL value. The MPCP model was created for BEM simulation. The simulated MPCP parameters were set to d = 0.9 mm, t = 1.3 mm, b = 5.64 mm and D = 9 mm. The results are presented in the frequency range of 200 Hz – 3.2 kHz. Subsequently, parametric studies of the MPCP concerning the perforation hole diameter, perforation ratio and depth of air space were carried out to investigate the acoustic performance.

3.2. Two-load measurement

On the basis of the BEM-simulated structure parameters, the prototype of the expansion chamber coupled MPCP was fabricated by 3D printing technology. Figure 5a shows the MPCP sample for TL measurement. The 3D printing material was polylactic acid of 1.3 $\mathrm{g/cm^3}$ density. An impedance tube with an inner diameter of 34.86 mm and the practical upper-frequency limit of 5500 Hz was used for the STL measurement setup, as shown in Fig. 5b. The sound pressure inside the tube was measured by four flush-

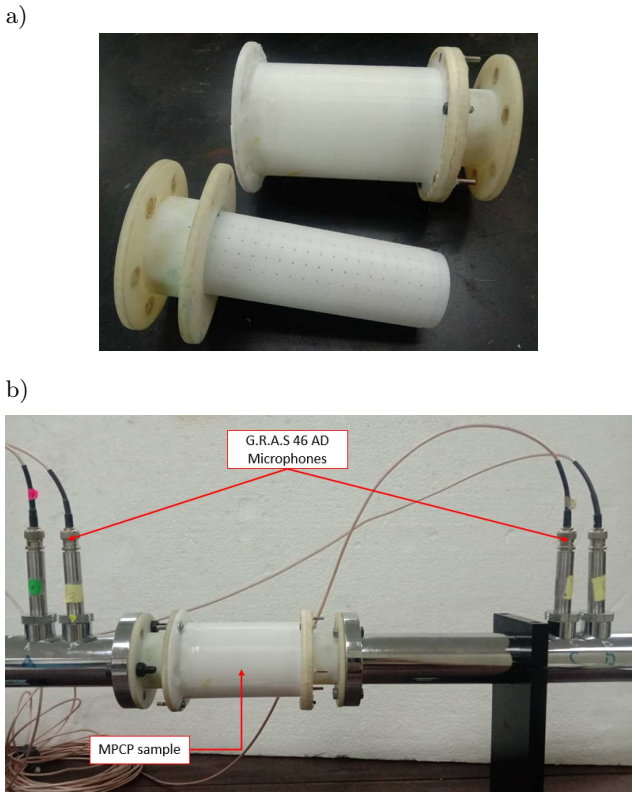

Fig. 5. a) 3D printed expansion chamber coupled MPCP; b) two-load method measurement set up.

mounted pressure microphones (G.R.A.S 46AD), LMS SCADAS system and LMS Test Lab software were utilised for the signal acquisition. The TL value of the proposed model was derived by an LMS Test Lab program following the two-load method.

3.3. RSM optimisation

Owing to the design consideration of the vacuum cleaner, the diameter D_1 is set to 31 mm and the axial lengths L_1 and L_2 were set to 50 mm and 30 mm, respectively. RSM optimisation via CCD was used in this study to find the optimum structure parameter for the expansion chamber coupled MPCP to maximise the TL at an objective frequency. The parameters were perforation diameter d, perforation spacing b, air cavity depth D_2, inlet unperforated length L_i and outlet unperforated length L_o. These five parameters were used to evaluate the response, which is the TL of the discussed model. The parameters of CCD were varied over three levels, between minimum (–1), midpoint, (0) and maximum (+1), as listed in Table 1. 50 CCD arrays were implemented to examine the five parameters, as in the following equation:

$$\mathrm{CCD} = 2^k + 2k + 6, \tag{11}$$

where k represents the parameter number. A mathematical model was established on the basis of the res-

Table 1. Actual and coded values for CCD.

Independent variables	Coded value		
	Minimum (−1), real value	Midpoint (0)	Maximum (+1)
Perforation diameter, d [mm]	0.6	0.8	1
Perforation ratio, σ [%]	2.5	3.1	4.3
Air cavity depth, D_2 [mm]	6	12	18
Inlet unperforated length, L_i [mm]	0	5	10
Outlet unperforated length, L_o [mm]	0	5	10

ponse to evaluate the minimal point through the quadratic model and given by

$$Y = \beta_0 + \int_{i=1}^{k} \beta_i X_i + \int_{i=1}^{k} \beta_{ij} X_i^2 + \int_{i\leq 1}^{k} \int_{i=1}^{k} \beta_i X_i X_j + \ldots + e, \quad (12)$$

where Y and $X_i X_j$ represent the response and variables, respectively. β_0, β_i, β_{ii}, and β_{ij} are the constant coefficient and interaction coefficients of the linear, quadratic and second-order terms. e is the random error.

3.4. Commercial vacuum cleaner analysis

A commercial vacuum cleaner was used in this study to investigate the practical attenuation effect of the discussed model. In general, the commercial vacuum cleaner was designed to include an air filter, quarter-wave tubes and Helmholtz resonators for noise control. Nonetheless, the noise attenuation was minimal when the area expansion ratio was constrained. Figure 6a illustrates the SPL measurement setup of the commercial vacuum cleaner investigated in this study. The measurement was carried out in a semi-anechoic

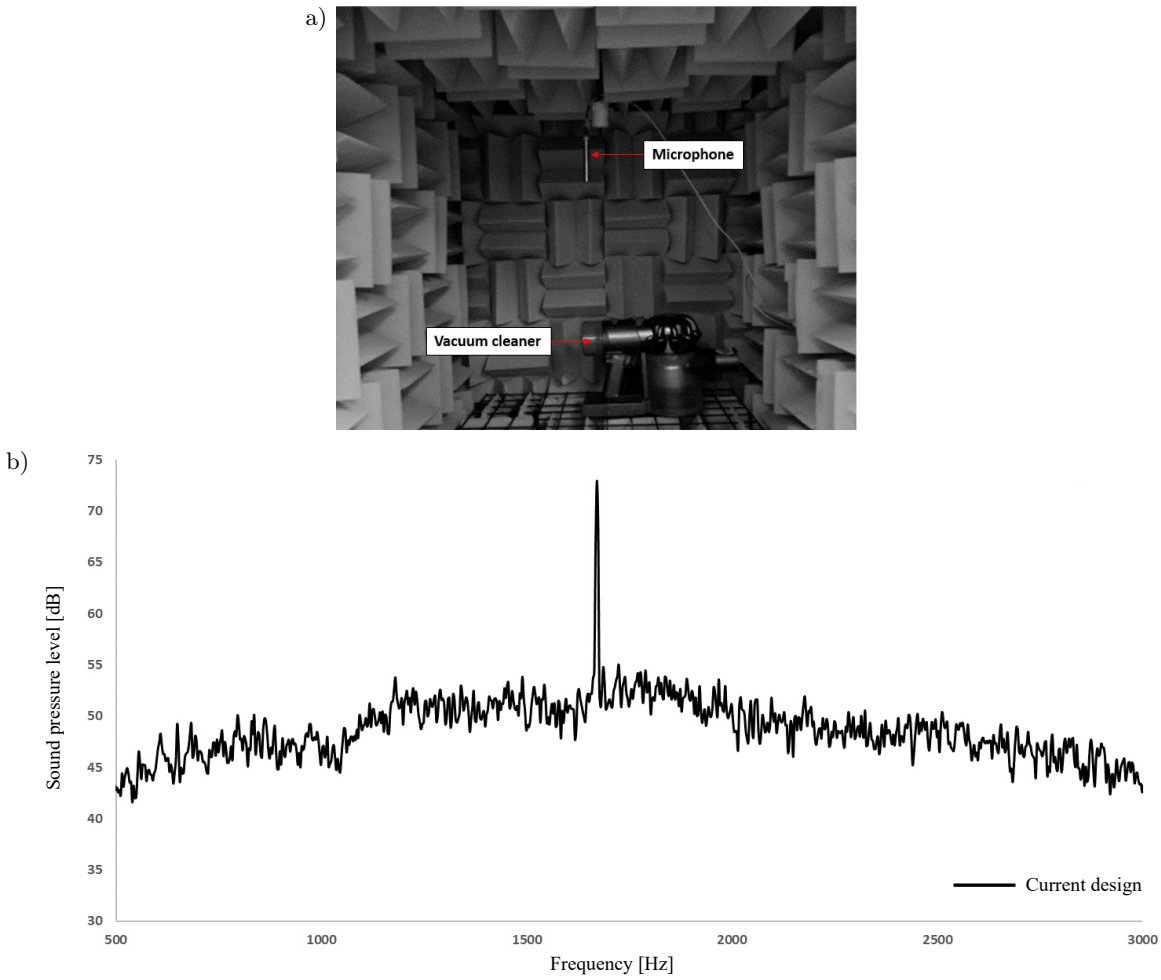

Fig. 6. a) Noise test bench of the commercial vacuum cleaner; b) vacuum noise behaviours under maximum working conditions.

chamber with 32.3 dB(A) background noise. A single microphone unit (G.RA.S 46 AD) coupled with LMS SCADAS data acquisition and LMS Test Express was used to measure the noise of the vacuum under maximum power working conditions. The microphone was approximately 300 cm from the vacuum exhaust. Figure 6b shows the SPL measurement set up of the vacuum noise under maximum working conditions. The figure shows that the vacuum noise contained the high narrow band in the frequency of 1.7 kHz. Thus, the expansion chamber coupled MPCP was applied here to attenuate the vacuum cleaner noise at 1.7 kHz.

4. Results

4.1. Model validation and parametric study

A comparison of the simulated TL-based BEM and measured TL from the impedance tube for the expansion chamber coupled MPCP is shown in Fig. 7. The solid blue line represents the simulated BEM results while the red dotted line is the measurement results. Both TL curves are shown to agree well and have a similar pattern of a dome shape with a TL peak at 2.55 kHz. The error between the BEM and the measured values is relatively small, and the R-square value is 0.89. However, the measured TL curve is broader along with the frequency compared to the simulated TL. The small deviation may be attributed to the inaccuracy of the parameters, such as actual air density, as reported in the study of Andersen (2008). Subsequently, the 3D-printed perforation holes are irregular (not perfectly circular) and produced burrs in actual condition. An imperfect condition on MPCP will influence the measured acoustic properties of MPCP and cause them to deviate from the simulation, as reported by Gaeta and Ahuja (2016).

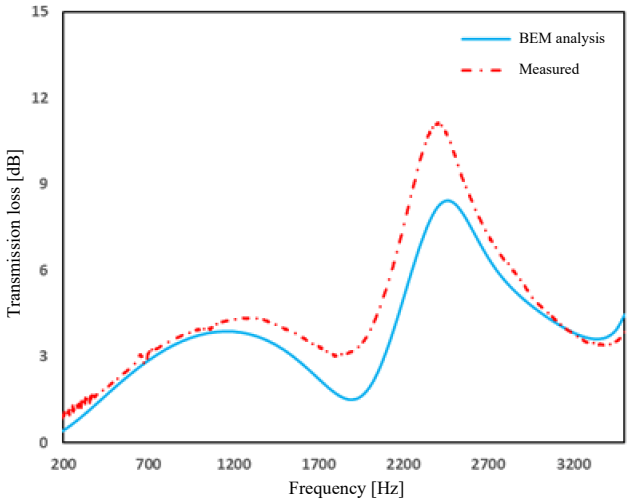

Fig. 7. Comparison of BEM analysis and two-load measurement results of the TL for the expansion chamber coupled MPCP model.

The effect of the perforation hole diameter is also studied via BEM according to the following: d = 0.9 mm, 0.7 mm, 0.5 mm, and 0.3 mm. The TL result is shown in Fig. 8a. The results show that the peak TL is shifted to the higher frequency and widens the attenuation peak. However, the peak value of TL is reduced based on the same configuration. As the perforation diameter is reduced, the acoustic resistance of the panel increases, causing the panel damping of the

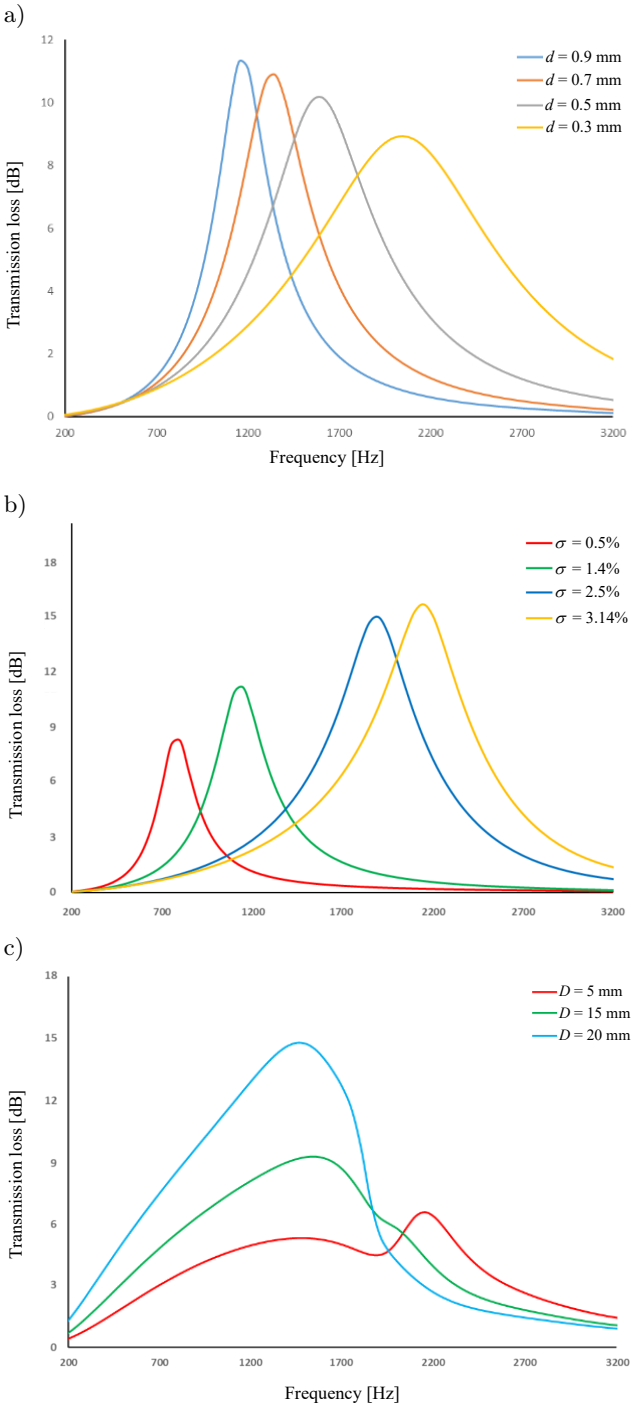

Fig. 8. Study of parametric effect of the MPCP: a) perforation hole diameter, b) perforation ratio, c) air cavity depth.

Helmholtz system to increase and the attenuation peak to widen (Wu, 1997).

Figure 8b shows the simulated TL of the expansion chamber coupled MPCP with the same configuration except for perforation ratio of σ = 0.5%, 1.4%, 2.5%, and 3.14%. The result shows that the peak TL is increased and shifts to a higher frequency. Moreover, as the percentage of porosity increases, it yields a higher TL over a wideband frequency. It is shown that the panel porosity can control the frequency where the peak TL happened. A proper selection of porosity value can improve the MPCP attenuation without significantly increasing the fabrication cost of reducing the perforation hole diameter or increasing the panel thickness.

The simulated TL of the expansion chamber coupled MPCP model with the same configuration, except for the air cavity depth, is shown in Fig. 8c, The air cavity depth is varied at 5, 15, and 20 mm. The result shows that one way to increase the TL amplitude is by increasing the air cavity depth. Only the fundamental TL amplitude decreases as the depth decreases while the peak frequency value of the TL remains almost constant.

4.2. Results of CCD optimisation

As listed in Table 2, 50 CCD batch runs are executed in this study. The objectives' function is to maximise the TL of the expansion chamber coupled MPCP (Y) at the frequency of 1.7 kHz. Table 2 depicts the highest TL (Y) of 21.64 dB when the perforation hole diameter is 1 mm, perforation ratio is 2.5% and air cavity depth is 18 mm with no axial length of inlet and outlet of unperforated segment implemented on the expansion model.

The best fitting of regression models for the TL (Y) is selected based on the highest-order polynomials, the significant additional terms and the absence of aliased models through the software. The accuracy of the quadratic model is improved considering the significant terms of 'Prob > F' are less than 0.05. Equation (12) shows the final empirical models in terms of code parameters (A – perforation hole diameter, B – perforation ratio, C – air cavity depth, D – inlet unperforated length and E – outlet unperforated length).

Table 3 shows the analysis of variance analysis for the model response Y. The quality of the model is assessed by R-squared (coefficient of determination),

Table 2. Results of the central composite design.

Run	Parameter (coded)					Response simulation
	A	B	C	D	E	Y
1	1	−1	−1	1	1	1.70469
2	0	0	1	0	0	20.6075
3	−1	−1	1	1	−1	14.6452
4	−1	−1	1	−1	−1	10.2393
5	−1	1	−1	1	1	4.82483
6	1	0	0	0	0	7.09251
7	−1	0	0	0	0	14.2055
8	−1	−1	1	−1	1	14.4479
9	−1	1	1	1	1	1.48093
10	−1	−1	−1	−1	−1	1.57126
11	0	0	0	0	0	10.4194
12	1	1	1	1	−1	12.429
13	0	0	−1	0	0	2.28554
14	−1	1	−1	−1	1	10.1884
15	−1	−1	−1	−1	1	1.85379
16	1	−1	1	1	1	11.5409
17	1	1	1	1	1	6.31351
18	0	0	0	0	0	10.4194
19	1	−1	−1	1	−1	1.57479
20	1	−1	−1	−1	1	1.42877
21	1	1	−1	−1	1	2.88269
22	1	−1	1	−1	−1	7.51056
23	0	0	0	0	0	10.4194
24	1	−1	−1	−1	−1	1.31233
25	0	0	0	−1	0	8.32391
26	0	−1	0	0	0	5.3692
27	1	−1	1	1	−1	9.0865
28	0	0	0	0	−1	8.44662
29	−1	1	−1	−1	−1	7.21091
30	−1	−1	−1	1	1	2.4626
31	−1	1	1	−1	1	2.44913
32	−1	−1	1	1	1	20.2239
33	0	0	0	1	0	14.2569
34	1	1	−1	1	−1	3.0075
35	0	0	0	0	0	10.4194
36	1	1	−1	1	1	5.15626
37	−1	1	1	−1	−1	3.829
38	1	1	1	−1	1	12.3233
39	0	0	0	0	0	10.4194
40	−1	1	−1	1	−1	10.2932
41	−1	−1	−1	1	−1	1.98024
42	0	0	0	0	0	10.4194
43	0	0	0	0	1	14.2255
44	−1	1	1	1	−1	2.44604
45	1	−1	1	−1	1	8.85659
46	1	1	1	−1	−1	21.6364
47	1	1	−1	−1	−1	2.01101
48	0	0	0	0	0	10.4194
49	0	0	0	0	0	10.4194
50	0	1	0	0	0	11.1041

Table 3. ANOVA for STL on MPCP (Y) with the independent variables.

Source	Sum of squares	DF	Mean square	F value	Prob > F
Model (Y)	1.99	20	0.0997	17.43	< 0.0001
A	0.0021	1	0.0021	0.3677	0.5490
B	0.0718	1	0.0718	12.56	0.0014
C	0.5248	1	0.5248	91.78	< 0.0001
D	0.0042	1	0.0042	0.7335	0.3988
E	0.0006	1	0.0006	0.0984	0.7560
AB	0.0539	1	0.0539	9.42	0.0046
AC	0.2203	1	0.2203	38.53	< 0.0001
AD	0.0138	1	0.0138	2.41	0.1314
AE	0.0102	1	0.0102	1.78	0.1930
BC	0.5647	1	0.5647	98.76	< 0.0001
BD	0.0242	1	0.0242	4.23	0.0489
BE	0.0155	1	0.0155	2.71	0.1104
CD	0.0437	1	0.0437	7.65	0.0098
CE	0.0289	1	0.0289	5.05	0.0324
DE	0.0037	1	0.0037	0.6428	0.4292
A^2	0.0003	1	0.0003	0.0514	0.8223
B^2	0.0046	1	0.0046	0.8130	0.3747
C^2	0.0543	1	0.0543	9.50	0.0045
D^2	2.884E–07	1	2.884E–07	0.0001	0.9944
E^2	5.093E–07	1	5.093E–07	0.0001	0.9925
Residual	0.1658	29	0.0057		
Lack of fit	0.1658	22	0.0075		
Pure error	0.0000	7	0.0000		
Std. dev	0.0756		R-squared	0.9232	
Mean	0.2330		Adj. R-squared	0.8703	
C.V	32.45		Pred. R-squared	0.7055	
PRESS	0.6361		Adeq. precision	18.0917	

The R^2 value is significantly high, which is 0.9232, and the standard deviation for this model is 0.0756.

$$\begin{aligned} Y = {} & 0.095386 + 0.00786397A - 0.0459532B - 0.124241C \\ & - 0.0111069D - 0.00406851E - 0.0410227AB \\ & - 0.0829731AC - 0.0207535AD - 0.0178171AE \\ & + 0.132844BC + 0.0274855BD + 0.0220128BE \\ & + 0.0369626CD + 0.0300391CE + 0.0107175DE \\ & + 0.0108973A^2 + 0.0433549B^2 + 0.148232C^2 \\ & + 0.000341448D^2 - 0.000453792E^2. \end{aligned} \tag{13}$$

Figure 9 illustrates the perturbation curve of the parameter sensitivity toward the response of TL. The depth of the air cavity is the most influential parameter compared to other parameters for the maximum TL. As described in Fig. 7c, air cavity depth has a significant effect on the amplitude of TL as the depth

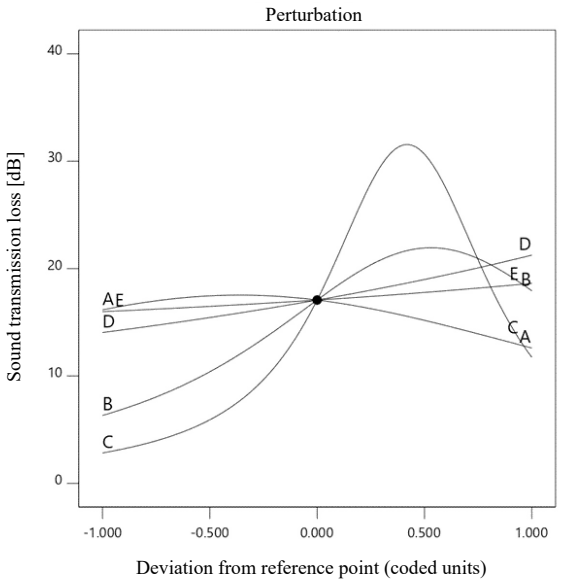

Fig. 9. Perturbation plot for a transmission loss.

is increased. The maximum TL decreases as the perforation hole diameter increases. Therefore, a large perforation diameter value should be avoided in the actual prototyping to sustain the maximum TL for the discussed expansion chamber MPCP.

The optimised structure parameters for the maximum TL of the expansion chamber coupled MPCP are obtained and listed in Table 4. The recommended optimised parameters are simulated using BEM and the solutions are compared with the RSM model responses listed in Table 5. The finding showed that reliable prediction could be attained through the suggested model

Table 4. Optimised structure parameters of the MPCP model.

Parameter	d [mm]	σ [%]	D [mm]	L_i [mm]	L_o [mm]
Optimized	0.86	2.5	15.5	9.91	0.31

Table 5. Model response and simulation validation.

	Response – transmission loss (Y)
Model response (CCD)	21.97
Simulation (BEM)	19.13

responses. In this study, the optimum values and interactive relationship of each parameter are successfully demonstrated using RSM. Optimised TL curve of the expansion chamber coupled MPCP model is shown in Fig. 10. The optimised model is shown to have a relatively good silencing property in the bandwidth of interest, which is 1.7 kHz.

4.3. Commercial vacuum cleaner noise test

The SPL of the vacuum cleaner attached with optimised MPCP is measured again for validation and the attenuation effect is investigated. Figure 11 illustrates

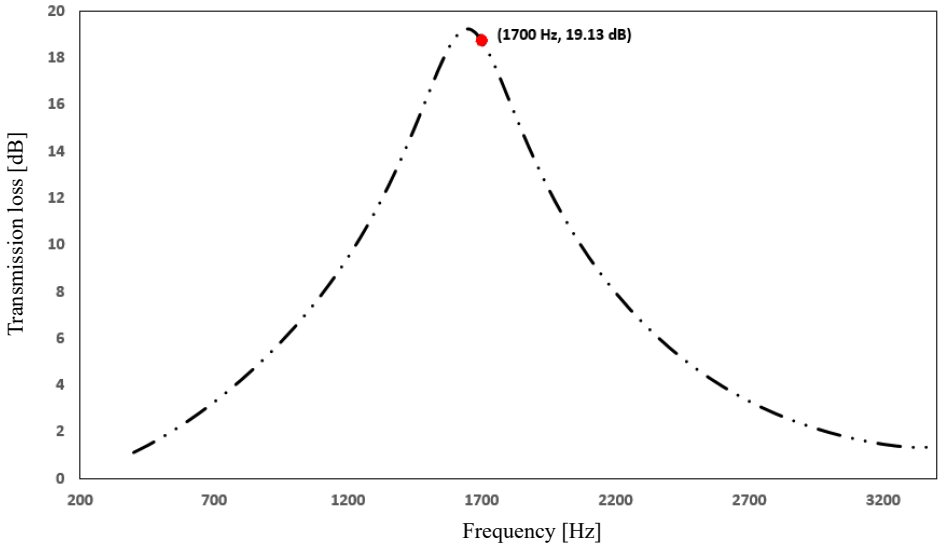

Fig. 10. Optimized transmission loss curve of expansion chamber coupled MPCP.

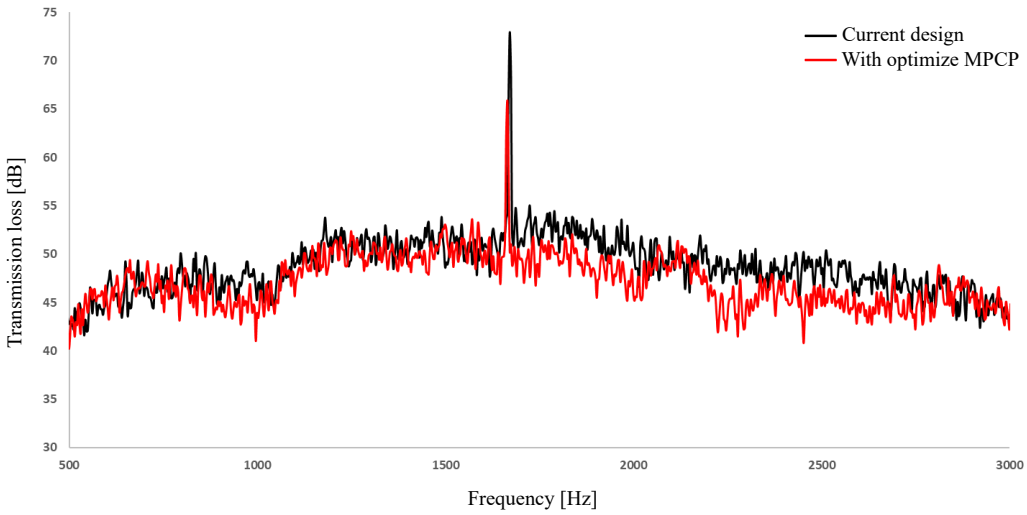

Fig. 11. Difference of sound pressure level of the current vacuum noise and with optimised MPCP model.

the SPL of the vacuum noise with and without the optimised MPCP. The A-weighted SPL of the vacuum noise is significantly reduced within the objective frequency after the optimised MPCP design is adopted. The outcome indicates that the proposed optimisation method is considered useful for the noise control application.

5. Conclusion

The acoustic performance of an expansion chamber coupled MPCP was investigated experimentally and numerically by a BEM approach. The simulated and measured results show good agreement with the R-square value of 0.89. The effect of different parameters, including perforation diameter, perforation ratio and depth of air cavity, on the acoustic behaviour of the expansion chamber coupled MPCP were also studied. The finding shows that reducing the perforation hole diameter is the most effective way to achieve wider peak attenuation. However, high porosity percentage was suitable to use for the high-frequency expansion chamber coupled MPCP applications. In addition, another way to increase the TL amplitude was by increasing the air cavity depth.

RSM optimisation of the expansion chamber coupled MPCP was likewise studied. The optimum values suggested were d = 0.86 mm, b = 2.5%, D = 15.5 mm, L_i = 9.91 mm, and L_o = 0.31 mm. The optimised MPCP was manufactured and applied to the vacuum. The vacuum SPL was shown to be significantly attenuated after the optimised expansion chamber coupled MPCP was adopted, and its A-weighted SPL was reduced significantly.

Acknowledgement

The authors would like to thank the Ministry of Higher Education of Malaysia, the Fundamental CREST Research Funds (304.PMEKANIK.6050379) and the Research Project of Vibration Laboratory of School of Mechanical Engineering for the support given to this research. The constructive comments from the anonymous reviewers are also acknowledged.

References

1. Andersen K.S. (2008), Analyzing muffler performance using the transfer matrix method, *Comsol Conference*, https://www.comsol.com/paper/analyzing-muffler-performance-using-the-transfer-matrix-method-5079.
2. Aziz M.S.A., Abdullah M.Z., Khor C.Y., Azid I.A. (2015), Optimization of pin through hole connector in thermal fluid–structure interaction analysis of wave soldering process using response surface methodology, *Simulation Modelling Practice and Theory*, **57**: 45–57, doi: 10.1016/j.simpat.2015.06.001.
3. Citarella R., Landi M. (2011), Acoustic analysis of an exhaust manifold by Indirect Boundary Element Method, *The Open Mechanical Engineering Journal*, **5**: 138–151, doi: 10.2174/1874155X01105010138.
4. Delany M.E., Bazley E.N. (1970), Acoustical properties of fibrous absorbent materials, *Applied Acoustics*, **3**(2): 105–116, doi: 10.1016/0003-682X(70)90031-9.
5. Fu J., Chen W., Tang Y., Yuan W., Li G., Li Y. (2015), Modification of exhaust muffler of a diesel engine based on finite element method acoustic analysis, *Advances in Mechanical Engineering*, **7**(4): 1687814015575954, doi: 10.1177/1687814015575954.
6. Gaeta R.J., Ahuja K.K. (2016), Effect of orifice shape on acoustic impedance, *International Journal of Aeroacoustics*, **15**(4–5): 474–495, doi: 10.1177/1475472X16642133.
7. Ganguli R. (2002), Optimum design of a helicopter rotor for low vibration using aeroelastic analysis and response surface methods, *Journal of Sound and Vibration*, **258**(2): 327–344, doi: 10.1006/jsvi.2002.5179.
8. Ishak M.H.H., Ismail F., Aziz M.S.A., Abdullah M.Z., Abas A. (2019), Optimization of 3D IC stacking chip on molded encapsulation process: a response surface methodology approach, *The International Journal of Advanced Manufacturing Technology*, **103**(1–4): 1139–1153, doi: 10.1007/s00170-019-03525-4.
9. Ji Z.L., Selamet A. (2000), Boundary element analysis of three-pass perforated duct mufflers, *Noise Control Engineering Journal*, **48**(5): 151–156, doi: 10.3397/1.2827962.
10. Kallias A.N., Imran Rafiq M. (2013), Performance assessment of corroding RC beams using response surface methodology, *Engineering Structures*, **49**: 671–685, doi: 10.1016/j.engstruct.2012.11.015.
11. Leong W.C., Abdullah M.Z., Khor C.Y. (2013), Optimization of flexible printed circuit board electronics in the flow environment using response surface methodology, *Microelectronics Reliability*, **53**(12): 1996–2004, doi: 10.1016/j.microrel.2013.06.008.
12. Li Z., Liang X. (2007), Vibro-acoustic analysis and optimization of damping structure with Response Surface Method, *Materials & Design*, **28**(7): 1999–2007, doi: 10.1016/j.matdes.2006.07.006.
13. Liu Z., Zhan J., Fard M., Davy J.L. (2017), Acoustic properties of multilayer sound absorbers with a 3D printed micro-perforated panel, *Applied Acoustics*, **121**: 25–32, doi: 10.1016/j.apacoust.2017.01.032.
14. Lu C., Chen W., Liu Z., Du S., Zhu Y. (2019), Pilot study on compact wideband micro-perforated muffler with a serial-parallel coupling mode, *Applied Acoustics*, **148**: 141–150, doi: 10.1016/j.apacoust.2018.12.001.
15. Maa D.Y. (1975), Theory and design of microperforated panel sound-absorbing constructions, *Scientia Sinica*, **18**(1): 55–71, doi: 10.1360/ya1975-18-1-55.

16. Munjal M.L. (1987), *Acoustics of Ducts and Mufflers with Application to Exhaust and Ventilation System Design*, John Wiley & Sons.

17. Na Y., Lancaster J., Casali J., Cho G. (2007), Sound absorption coefficients of micro-fiber fabrics by reverberation room method, *Textile Research Journal*, **77**(5): 330–335, doi: 10.1177/0040517507078743.

18. Qian Y.J., Kong D.Y., Liu S.M., Sun S.M., Zhao Z. (2013), Investigation on micro-perforated panel absorber with ultra-micro perforations, *Applied Acoustics*, **74**(7): 931–935, doi: 10.1016/j.apacoust.2013.01.009.

19. Qin X., Wang Y., Lu C., Huang S., Zheng H., Shen C. (2016), Structural acoustics analysis and optimization of an enclosed box-damped structure based on response surface methodology, *Materials & Design*, **103**: 236–243, doi: 10.1016/j.matdes.2016.04.063.

20. C S.W. *et al.* (2019), Improvement of the sound absorption of flexible micro-perforated panels by local resonances, *Mechanical Systems and Signal Processing*, **117**: 138–156, doi: 10.1016/j.ymssp.2018.07.046.

21. Selamet A., Ji Z.L. (1999), Acoustic attenuation performance of circular expansion chambers with extended inlet/outlet, *Journal of Sound and Vibration*, **223**(2): 197–212, doi: 10.1006/jsvi.1998.2138.

22. Selamet A., Ji Z.L., Radavich P.M. (1998), Acoustic attenuation performance of circular expansion chambers with offset inlet/outlet: II. Comparison with experimental and computational studies, *Journal of Sound and Vibration*, **213**(4): 619–641, doi: 10.1006/jsvi.1998.1515.

23. Tan W.-H., Ripin Z.M. (2013), Analysis of exhaust muffler with micro-perforated panel, *Journal of Vibroengineering*, **15**(2): 558–573.

24. Tan W.-H., Ripin Z.M. (2016), Optimization of double-layered micro-perforated panels with vibro-acoustic effect, *Journal of the Brazilian Society of Mechanical Sciences and Engineering*, **38**(3): 745–760, doi: 10.1007/s40430-014-0274-4.

25. Vasile O. (2010), Transmission loss assessment for a muffler by boundary element method approach, *Analele Universităţii "Eftimie Murgu"*, **17**(1): 233–242, http://anale-ing.uem.ro/2010/26_C.pdf.

26. Wang Y., Qin X., Huang S., Lu L., Zhang Q., Feng J. (2017), Structural-borne acoustics analysis and multi-objective optimization by using panel acoustic participation and response surface methodology, *Applied Acoustics*, **116**: 139–151, doi: 10.1016/j.apacoust.2016.09.013.

27. Wu M.Q. (1997), Micro-perforated panels for duct silencing, *Noise Control Engineering Journal*, **45**(2): 69–77.

28. Yuksel E., Kamci G., Basdogan I. (2012), Vibro-acoustic design optimization study to improve the sound pressure level inside the passenger cabin, *Journal of Vibration and Acoustics*, **134**(6): 061017-1–061017-9, doi:10.1115/1.4007678.

29. Zhenlin J., Qiang M., Zhihua Z. (1994), Application of the boundary element method to predicting acoustic performance of expansion chamber mufflers with mean flow, *Journal of Sound and Vibration*, **173**(1): 57–71, doi: 10.1006/jsvi.1994.1217.